Journal of Sound and Vibration 326 (2009) 870–882

Contents lists available at ScienceDirect

Journal of Sound and Vibration

journal homepage: www.elsevier.com/locate/jsvi

Suppression of time aliasing in the solution of the equations of motion of an impacted beam with partial constrained layer damping

Jean-François Blais [a,1], Massimo Cimmino [b], Annie Ross [b,*], Daniel Granger [c]

[a] Bombardier Aerospace, P.O. Box 6087, Station Centre-Ville, Montréal, Québec, Canada, H3C 3G9
[b] CREPEC, Department of Mechanical Engineering, École Polytechnique de Montréal, P.O. Box 6079 station Centre-ville, Montréal, Québec, Canada H3C 3A7
[c] Alstom Hydro Canada, 1350 ch., Saint-Roch, Sorel-Tracy, Québec, Canada J3R 5P9

ARTICLE INFO

Article history:
Received 1 November 2008
Received in revised form
16 May 2009
Accepted 1 June 2009
Handling Editor: C.L. Morfey
Available online 16 July 2009

ABSTRACT

Signal processing issues encountered when an analytical spectrum is converted in the time domain with an inverse discrete Fourier transform are investigated. In the analytical model of the transient time response of an impacted beam with partial constrained layer damping (PCLD) developed in Ref. [D. Granger, A. Ross, Effects of partial constrained viscoelastic layer damping parameters on the initial transient response of impacted cantilever beams: experimental and numerical results, *Journal of Sound and Vibration* 321 (1–2) (2009) 45–64, doi:10.1016/j.jsv.2008.09.039], noncausal effects were observed for lightly damped structures. As discussed in the present paper, the noncausal effects were due to time aliasing occurring when continuous frequency spectra were discretized. To suppress such errors, the numerical Laplace transform is introduced and applied to the previous model, which was based on Fourier transforms. The equations of motion of the system and the viscoelastic properties of the core are formulated in the Laplace domain. A window is used in the Laplace domain to avoid amplification of the Gibbs oscillations that are caused by the truncation of the spectrum. The new solution technique is compared to the previous method. It is shown that noncausal effects appearing in the first milliseconds of time signals with the use of discrete Fourier transforms are avoided with the Laplace transform solution method. Numerical results are validated for transient responses using experimental impact force signals. The results are in good agreement with experimental data.

1. Introduction

Transient responses of impacted structures are a source of concern, especially when dealing with occupational health. Many manufacturing processes, such as riveting, are based on mechanical impacts. Strong impacts induce significant transient vibrations and powerful transient noises that can undoubtedly cause hearing impairment. Sound production is particularly strong with large, flexible impacted structures. Both the lack of effectiveness of auditory protection equipments and the reluctance of workers to use them can result in hearing injuries. Therefore, partial constrained layer damping

Abbreviations: a.u., arbitrary units; CLD, constrained layer damping; DFT, discrete Fourier transform; dof, degree of freedom; EOM, equations of motion; FFT, fast Fourier transform; FRF, frequency response function; NLT, numerical Laplace transform; PCLD, partial constrained layer damping.

* Corresponding author. Tel.: +1 514 340 4711; fax: +1 514 340 4176.
E-mail address: annie.ross@polymtl.ca (A. Ross).

[1] This work was done while the author was affiliated with the École Polytechnique de Montréal.

0022-460X/$ - see front matter © 2009 Elsevier Ltd. All rights reserved.
doi:10.1016/j.jsv.2009.06.001

(PCLD) is sometimes used to reduce vibrations and, thus, the radiated noise. PCLD consists of a viscoelastic layer topped with a constraining elastic layer that both cover part of the structure. PCLD can be applied to existing structures, and was shown to be quite efficient when compared to complete constrained layer damping (CLD) [1].

Impact noises are partly due to the initial transient motion of structures [2–4]. Damping treatments designed to reduce such vibrations would therefore greatly benefit from the modeling for transient time response of impacted mechanical structures. Granger and Ross presented an analytical model of the time domain dynamics of PCLD treated beams [5]. Beams were used as a basic structure to understand the behavior of more complex structures. In this model, the viscoelastic properties of the core were nonlinear and the shear modulus was modeled using a Prony series in the Fourier domain. The equations of motion (EOM) of the system were obtained using Lagrange's equations. The EOM were converted in the frequency domain using a Fourier transform, and were solved for frequency displacements using the assumed modes method. The displacements were then converted back in the time domain using inverse discrete Fourier transforms (DFT). The excitations used were experimental force signals. Time responses were shown to be in fairly good agreement with experimental data, for various PCLD parameters.

It was shown, however, that responses calculated using the analytical model and solution method were noncausal for systems with poor damping ratios. This was explained by the fact that the time signals for lightly damped beams remained significant at the end of the calculation period, causing time aliasing in the solution process.

In order to extend the applicability of the model to any damping ratio, the present paper discusses time aliasing and Gibbs oscillations, two phenomena encountered when analytical spectra are inverted numerically. The numerical Laplace transform (NLT) and windowing in the frequency domain are introduced to significantly reduce these signal processing issues. The model used by Granger and Ross is thus reformulated using a Laplace transform approach in order to avoid noncausal effects and produce reliable initial transient responses. The response can be used in parametric studies of PCLD treatments, regardless of the damping ratio of the system. Both formulations in the Fourier and the Laplace domains are compared using experimental force signals and different PCLD configurations. Finally, the model developed in the Laplace domain is validated experimentally.

2. Numerical inversion of an analytical spectrum

The method developed by Granger and Ross did produce interesting results, but lead to inaccuracies at the very beginning of the time response signals. The authors stated that these noncausal displacements resulted from the use of discrete Fourier transforms to invert the frequency response function (FRF) of PCLD beams. The magnitude of the error was significant for signals that were not sufficiently damped by the end of the observation window. Fig. 1 shows an example of the initial transverse displacement of an impacted beam for two configurations for which damping ratios differ. It is seen in this figure that the time signal corresponding to the beam configuration that is highly damped (——) is causal while the other signal (— - —) is not. Such problem occurred even though simulations were run over 26 s, which cost enormous computing time and memory allocation. It will now be shown how the noncausal displacements are created during the inverse discrete Fourier transform operation.

The inverse DFT is written as

$$f_n = \frac{\Delta\omega}{2\pi} \sum_{q=-N/2}^{N/2-1} F_q \, e^{i2\pi qn/N}, \tag{1}$$

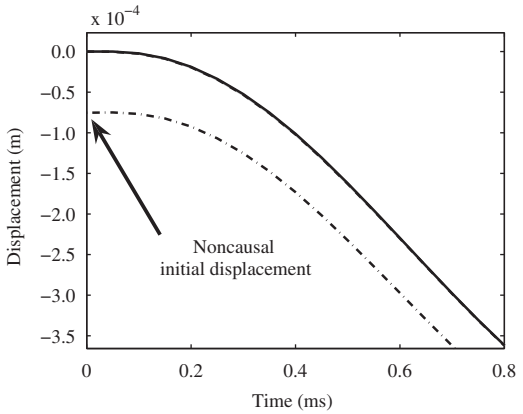

Fig. 1. Example of inaccuracy at the beginning of simulated beam displacements [5]: high (——) and low (— - —) damping.

where F_q is a an arbitrary sampled spectrum, $\Delta\omega$ is the frequency step, N is the number of points in the spectrum, and n and q are integers. Two processes are involved in the inverse DFT. First, an arbitrary continuous spectrum $F(\omega)$ is being discretized to form F_q. Second, the sampled spectrum is being truncated from $\omega = -N\Delta\omega/2$ to $(N-1)\Delta\omega/2$.

To understand how these two processes affect the resulting time signal, let us first consider the analytical expression of the inverse continuous Fourier transform $\mathscr{F}^{-1}$ of a given spectrum $F(\omega)$, i.e.

$$\mathscr{F}^{-1}\{F(\omega)\} = f(t) = \frac{1}{2\pi}\int_{-\infty}^{+\infty} F(\omega)\,\mathrm{e}^{\mathrm{i}\omega t}\,\mathrm{d}\omega, \tag{2}$$

where $f(t)$ is the corresponding signal in the time domain. Both the discretization and the truncation processes can be also represented by analytical functions.

First, the discretization of the continuous spectrum $F(\omega)$ with a frequency step $\Delta\omega$ can be described analytically by the Dirac comb function given by

$$\mathit{\Pi\!\Pi}(\omega,\Delta\omega) = \Delta\omega\sum_{q=-\infty}^{+\infty}\delta(\omega - q\,\Delta\omega), \tag{3}$$

where q is an integer.

Second, the truncation of $F(\omega)$ can be represented analytically by a rectangular window function given by

$$\mathit{\Pi}(\omega,\Omega) = \begin{cases} 1, & |\omega| \le \Omega, \\ 0, & |\omega| > \Omega, \end{cases} \tag{4}$$

where Ω is the cutoff frequency of the window. This frequency is chosen in such way that no critical spectral information is being lost in the windowing process.

Therefore, it is possible to write Eq. (1) over a continuous time t in terms of Eqs. (2)–(4), i.e.

$$\tilde{f}(t) = \frac{1}{2\pi}\int_{-\infty}^{+\infty} F(\omega)\,\underbrace{\mathit{\Pi\!\Pi}(\omega,\Delta\omega)}_{\text{Discretization}}\,\underbrace{\mathit{\Pi}(\omega,\Omega)}_{\text{Truncation}}\,\mathrm{e}^{\mathrm{i}\omega t}\,\mathrm{d}\omega. \tag{5}$$

We now propose to study independently functions $\mathit{\Pi\!\Pi}$ and $\mathit{\Pi}$, and their consequences in the time domain. The continuous time function $\tilde{f}_D(t)$ resulting from the discretization of the spectrum can be written as

$$\tilde{f}_D(t) = \frac{1}{2\pi}\int_{-\infty}^{+\infty} F(\omega)\mathit{\Pi\!\Pi}(\omega,\Delta\omega)\,\mathrm{e}^{\mathrm{i}\omega t}\,\mathrm{d}\omega. \tag{6}$$

In the time domain, the discretization of the spectrum is reflected by expressing Eq. (6) in terms of a convolution integral $(*)$, i.e.

$$\tilde{f}_D(t) = f(t) * \mathscr{F}^{-1}\{\mathit{\Pi\!\Pi}(\omega,\Delta\omega)\}. \tag{7}$$

The inverse Fourier transform of the discretization function $\mathit{\Pi\!\Pi}$ is

$$\mathscr{F}^{-1}\{\mathit{\Pi\!\Pi}(\omega,\Delta\omega)\} = \sum_{m=-\infty}^{+\infty}\delta(t - mT_{\max}), \tag{8}$$

where $T_{\max} = 2\pi/\Delta\omega$ and m is an integer. By combining Eqs. (7) and (8), $\tilde{f}_D(t)$ can be written as

$$\tilde{f}_D(t) = \sum_{m=-\infty}^{+\infty} f(t - mT_{\max}). \tag{9}$$

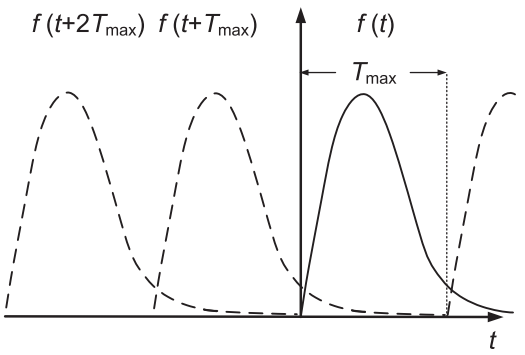

Fig. 2. Periodization of the time function $f(t)$ due to inverse DFT.

Hence, the consequence of discretizing the spectrum is the replication of the time signal $f(t)$ with a period $T_{\max}$. Assuming that the duration of $f(t)$ is longer than $T_{\max}$, this results in an overlap of the periodic replications of the time signal, as illustrated in Fig. 2. The signal obtained inside an observation window $0 \le t \le T_{\max}$ is a summation of the actual signal and the various replications appearing in the observation window. This phenomenon is called time aliasing, and it causes considerable errors if the amplitude of $f(t)$ is significant for $t > T_{\max}$.

The second issue related to the inverse DFT is the truncation of the spectrum. The continuous time function $\tilde{f}_T(t)$ resulting from the truncation of $F(\omega)$ can be written as

$$\tilde{f}_T(t) = \frac{1}{2\pi}\int_{-\infty}^{+\infty} F(\omega)\Pi(\omega,\Omega)\,\mathrm{e}^{\mathrm{i}\omega t}\,\mathrm{d}\omega. \tag{10}$$

In the time domain, Eq. (10) becomes

$$\tilde{f}_T(t) = f(t) * \mathscr{F}^{-1}\{\Pi(\omega,\Omega)\}. \tag{11}$$

The inverse Fourier transform of the truncation function Π is

$$\mathscr{F}^{-1}\{\Pi(\omega,\Omega)\} = \frac{\Omega}{\pi}\mathrm{sinc}(\Omega t), \tag{12}$$

where sinc is the cardinal sine function. Consequently, by combining Eqs. (11) and (12), $\tilde{f}_T(t)$ is given by

$$\tilde{f}_T(t) = f(t) * \frac{\Omega}{\pi}\mathrm{sinc}(\Omega t). \tag{13}$$

In the time domain, oscillations at the frequency Ω can occur due to the sinc function. The oscillations are canceled out wherever $f(t)$ and its derivative are continuous, due to the convolution process. However, fast oscillations are not canceled out and appear in the time signal if the amplitude or the slope of the signal have discontinuities. This time effect related to the truncation of the spectrum is known as the Gibbs phenomenon. The amplitude of these oscillations decreases on both sides of a discontinuity as does the amplitude of the sinc function when $|t|$ increases. This means that some of the energy contained in the analytical FRF leaks to both sides of the time domain discontinuities when the spectrum is truncated. For instance, Gibbs oscillations are visible when a Fourier spectrum representing periodic square pulses is truncated.

Moreover, even though discretization and truncation of the spectrum were presented independently, they both can occur simultaneously. Hence, the continuous time function $\tilde{f}(t)$ in Eq. (5) is written as

$$\tilde{f}(t) = \underbrace{\sum_{m=-\infty}^{+\infty} f(t - mT_{\max})}_{\text{Time aliasing}} * \underbrace{\frac{\Omega}{\pi}\mathrm{sinc}(\Omega t)}_{\text{Gibbs phenomenon}}. \tag{14}$$

Consequently, the Gibbs phenomenon does not only affect the time signal $f(t)$, but it also affects its replications.

Finally, time aliasing and Gibbs oscillations were introduced with a continuous time signal $\tilde{f}(t)$. However, since DFT and inverse DFT algorithms are reciprocal, inversion of a continuous spectrum using Eq. (1) with fixed parameters $\Delta\omega$ and Ω lead to a time signal that is also discretized and truncated, with a time step $\Delta t = \pi/\Omega$ and an observation window of length $T_{\max}$. The resulting discretized and finite time signal is related to the continuous signal in Eq. (14), and is given by $f_n = \tilde{f}(n\Delta t)$, with $0 \le n \le N-1$.

As an example of time aliasing, let us now consider the analytical frequency response function of a single degree of freedom (dof) system

$$H(\overline{\Omega}) = \frac{1}{k}\frac{1}{(1-\overline{\Omega}^2) + 2\mathrm{i}\zeta\overline{\Omega}}, \tag{15}$$

where k and ζ are, respectively, the stiffness and the damping ratio of the system. The nondimensional frequency is $\overline{\Omega} = \omega/\omega_n$, where ω_n is the natural frequency of the system. The envelope of the impulse response that corresponds to Eq. (15) may be significant at all times included within $0 \le t \le +\infty$. Therefore, it may be significant at $t > T_{\max}$ and hence, time aliasing may occur, as explained previously.

Fig. 3 shows the analytical impulse response (——) of an arbitrary single dof system with $\zeta = 1$ percent, $k = 25\,\mathrm{N/m}$, and $\omega_n = 5\,\mathrm{rad/s}$. It is compared to the impulse response obtained using the inverse DFT on the discrete FRF of the system (– – –). The discretization and truncation parameters of the spectrum were chosen as $\Delta\omega = 2\pi/15$ and $\Omega = 100\pi\,\mathrm{rad/s}$. The two signals are obviously different. The amplitude is roughly 50 percent higher with the inverse DFT. A small phase lag can be observed, causing the impulse response to begin with a value of -0.1 a.u. when the inverse DFT is applied. The amplitude error and phase shift due to aliasing depend on the sampling parameters of the FRF. This example illustrates how the inverse DFT can create noncausal displacement and errors over the entire observation window when applied for the solution of an EOM defined in the frequency domain.

One should note that the Gibbs oscillations are not visible in this particular case. As it was seen previously, this phenomenon occurs only when discontinuities or sharp amplitude changes are encountered in the time signal. Due to the weak damping ratio chosen to illustrate the consequences of the periodic replications in Fig. 3, the time signal and its

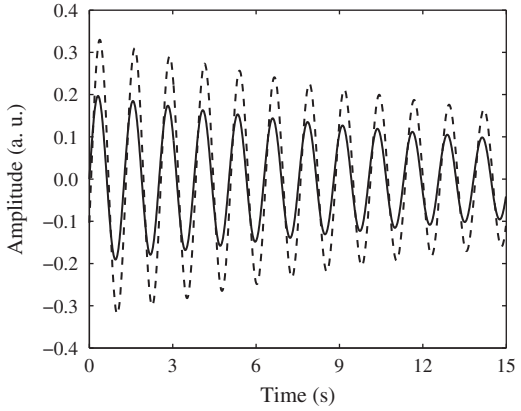

Fig. 3. Impulse response: analytical (———) and calculated using the inverse DFT (— - —).

derivative are practically continuous between $t = T^{-}_{\max}$ and $T^{+}_{\max}$. Therefore, the amplitude of the Gibbs oscillations is negligible compared to the amplitude of the time signal resulting from the inverse DFT.

To overcome time aliasing, the solution proposed by Granger and Ross was to increase the simulation time to enormous proportions with respect to the observation window. A longer simulation time yielded a lower signal amplitude at the end of the observation window. For this purpose, the frequency step $\Delta\omega$ was reduced, since $T_{\max} = 2\pi/\Delta\omega$. However, increasing $T_{\max}$ required more computing time. We will see in the next sections that replacing DFTs by numerical Laplace transforms can considerably reduce time aliasing errors without requiring enormous simulation time with respect to the duration of the observation window. Nevertheless, the Gibbs phenomenon must also be treated carefully in the Laplace domain.

3. Numerical Laplace transform

The Laplace transform has proved to be an efficient tool to study transient phenomena. It is commonly used in control systems. To overcome difficulties encountered in the inversion of Laplace transforms, Wilcox introduced the numerical Laplace transform [6]. Since then, the NLT has been successfully applied to several fields such as electrical transmission lines [6–8], vibrations [9–12], and acoustics [13,14]. For instance, Ni et al. combined the NLT to the pseudo-force method to analyze the nonlinear transient response of a suspended cable subjected to an arbitrary dynamic load [12].

3.1. Formulation of the NLT

The analytical Laplace transform and its inverse are defined as follow:

$$\mathscr{L}\{f(t)\} = L(s) = \int_0^{+\infty} f(t)\,\mathrm{e}^{-st}\,\mathrm{d}t, \tag{16}$$

$$\mathscr{L}^{-1}\{L(s)\} = f(t) = \frac{1}{2\pi\mathrm{i}}\int_{\sigma-\mathrm{i}\infty}^{\sigma+\mathrm{i}\infty} L(s)\,\mathrm{e}^{st}\,\mathrm{d}s, \tag{17}$$

with $s = \sigma + \mathrm{i}\omega$ and where σ is an artificial damping factor. For real, causal signals, Eqs. (16) and (17) can be rewritten as

$$L(\sigma + i\omega) = \int_{-\infty}^{+\infty} f(t)\,\mathrm{e}^{-(\sigma+\mathrm{i}\omega)t}\,\mathrm{d}t = \int_{-\infty}^{+\infty} [f(t)\,\mathrm{e}^{-\sigma t}]\,\mathrm{e}^{-\mathrm{i}\omega t}\,\mathrm{d}t, \tag{18}$$

$$f(t) = \frac{1}{2\pi}\int_{-\infty}^{+\infty} L(\sigma + \mathrm{i}\omega)\,\mathrm{e}^{(\sigma+\mathrm{i}\omega)t}\,\mathrm{d}\omega = \frac{e^{\sigma t}}{2\pi}\int_{-\infty}^{+\infty} L(\sigma + \mathrm{i}\omega)\,\mathrm{e}^{-\mathrm{i}\omega t}\,\mathrm{d}\omega. \tag{19}$$

Knowing that the analytical Fourier transform is defined as

$$\mathscr{F}\{f(t)\} = F(\omega) = \int_{-\infty}^{+\infty} f(t)\,\mathrm{e}^{-\mathrm{i}\omega t}\,\mathrm{d}t \tag{20}$$

and its inverse was defined in Eq. (2), then Eqs. (18) and (19) become

$$L(\sigma + \mathrm{i}\omega) = \mathscr{F}\{f(t)\,\mathrm{e}^{-\sigma t}\}, \tag{21}$$

$$f(t) = \mathrm{e}^{\sigma t}\,\mathscr{F}^{-1}\{L(\sigma + \mathrm{i}\omega)\}. \tag{22}$$

Hence, the numerical Laplace transform can be implemented in Matlab by means of the fast Fourier transform (FFT) algorithm.

3.2. Selection of σ

The real part of the Laplace variable (σ) must be set in order to use standard FFT procedures. The value of σ is set according to two criteria described below. First, in Eq. (21), σ acts as an artificial damping factor on the time signal, as long as its value is positive. The greater σ is, the more damped the time signal becomes, and therefore, the causality errors due to the discretization of the spectrum are reduced. In fact, replications still overlap with the studied time signal in the interval $0 \leq t \leq T_{\max}$, but their amplitudes are several orders of magnitude lower (i.e. $e^{-\sigma T_{\max}} \ll e^{0}$). However, in Eq. (22), a positive σ leads to a reconstructed signal $f(t)$ that increases exponentially with time. If the value of σ is great, the smallest residual signal at the end of the observation window will thus explode, leading to unrealistic results. The selection of σ is made of a compromise between the need to damp the time signal and the need to limit the numerical instability.

Different authors have proposed ways to set parameter σ. The most common ones are presented in Table 1. In all cases, the longer is the time signal, the less damping is required. This brings us back to the previous statement: increasing the duration of the time signal reduces the causality error. In addition, Wedepohl proposed a relationship with N, the number of points in the time signal [7]. Given a value of $T_{\max}$, the sampling frequency ω_s is higher for a larger value of N. Therefore, the truncation of the spectrum is less significant and the value of σ can be set higher. In the present work, the Wedepohl parameter is used.

3.3. Reduction of the Gibbs phenomenon

As it was previously seen, the Gibbs phenomenon appears at sharp amplitude changes in a given time signal. Hence, oscillations at frequency Ω may be observed. In the case of a damped oscillating time signal resulting from the inversion of a discretized and truncated spectrum, discontinuities are likely to occur at the beginning and at the end of the time period.

The Gibbs phenomenon is particularly problematic when an inverse Laplace transform is applied to the truncated spectrum: the high frequency ripples at the end of the time signal become over amplified due to the exponential term ($e^{\sigma t}$) in Eq. (22). Fig. 4 illustrates the amplified Gibbs phenomenon on an arbitrary time signal with a discontinuity. A time signal (– – –) is shown with a discontinuity at $t = 17$ ms. The time signal obtained from the inverse NLT of the corresponding truncated spectrum (———) contains oscillations of increasing amplitude near the discontinuity. These high frequency ripples can be observed over a relatively long time prior to the discontinuity. However, Gibbs oscillations at the vicinity of $t = 0$ are not amplified since the exponential term in Eq. (22) is unitary at this time.

Table 1
Functions proposed to set the value of σ.

Author	Proposed σ
Wilcox [6]	$2\pi/T_{\max}$
Wedepohl [7]	$2\ln(N)/T_{\max}$
Krings and Waller [9]	$10/T_{\max} \leq \sigma \leq 3/T_{\max}$

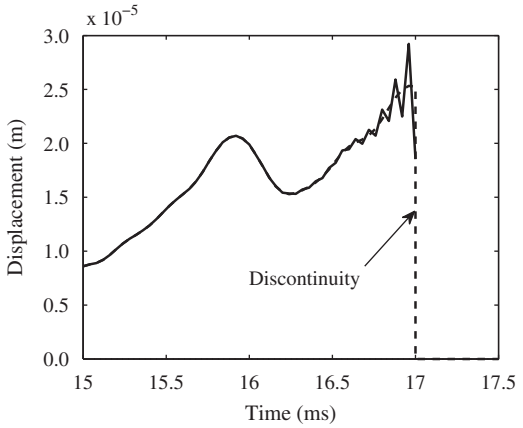

Fig. 4. Amplified Gibbs phenomenon: arbitrary time signal (– – –) and time signal from the inverse NLT (———).

There are two ways to reduce the effects of the Gibbs phenomenon. The first one is to increase the sampling frequency so that truncation of the spectrum is less significant. However, this is not always possible experimentally, since sampling frequency is limited by the acquisition device. In the case of simulated signals, time steps are limited by the computer resources, so the sampling frequency cannot be increased infinitely. A compromise must be reached to obtain a proper time signal with acceptable computer time and memory.

Windowing in the frequency domain was introduced as a second way to reduce the Gibbs phenomenon [15]. The rectangular window given by Eq. (4) and applied to the frequency spectrum can be replaced by other windows to reduce the truncation effect. Several windows such as Hanning, Blackman, Lanczos, and Riesz were studied by Ramirez et al. [8]. However, the amplitudes of such windows decrease rapidly in the spectrum and this is not suitable for broadband signals such as impact response signals. It would lead to a significant attenuation of high frequency components which would be detrimental to the recovery of the initial time signal. A Tukey window can be used as a trade-off between Hanning and rectangular windows. It is defined as [16]

$$\Gamma(q)=\begin{cases}1, & |q|<\dfrac{N}{2}-Q,\\ \dfrac{1}{2}\left[1-\cos\left(\dfrac{\pi\left(|q|-\dfrac{N}{2}\right)}{Q}\right)\right], & \dfrac{N}{2}-Q\le|q|\le\dfrac{N}{2},\end{cases} \tag{23}$$

where $N/2$ is the maximum value taken by q and Q is the width of the tapered rim. In the present work, the width of the tapered rim is set in such a way that $2Q/N=30$ percent.

It is therefore proposed to present the EOM of the PCLD treated beam in the Laplace domain, in order to obtain a causal response for systems with any amount of damping.

4. PCLD beam model in the Laplace domain

Although the baseline model was fully presented by Granger and Ross [5], the model is briefly described in this section in order to present and outline the particularities pertaining to the application of the Laplace transforms.

4.1. Geometry

The system consists of a homogeneous, uniform beam of length L_0 and arbitrary boundary conditions, padded with a partial constrained viscoelastic layer. In Fig. 5, the base beam is cantilevered. The damping treatment of length L_c is composed of two layers and is installed from x_1 to x_2, where x is the axial coordinate of the beam. Each layer has a thickness h_β and a density ρ_β, where $\beta=b$, v, or c for the base beam, the viscoelastic layer, and the constraining layer, respectively. The system has a uniform width B. The force is applied at x_f, and x_0 indicates the location where the response of the system is measured (not shown in Fig. 5). The mechanical and physical assumptions for the model were presented by Granger and Ross [5].

The system displacements are defined as follow, and are shown in Fig. 6:

1. $w(x,t)$ is the transverse displacement of the system along the z-axis;
2. $u_b(x,t)$ is the longitudinal displacement of the base beam along the x-axis; and
3. $u_c(x,t)$ is the longitudinal displacement of the constraining layer along the x-axis.

4.2. Viscoelastic shear modulus

Viscoelastic shear properties are frequency dependent [17]. In the present work, accurate representation of the core layer both in the frequency and time domains is obtained by using Prony series to represent the viscoelastic properties. The

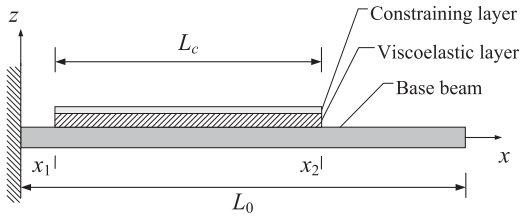

Fig. 5. Base beam with viscoelastic PCLD [5].

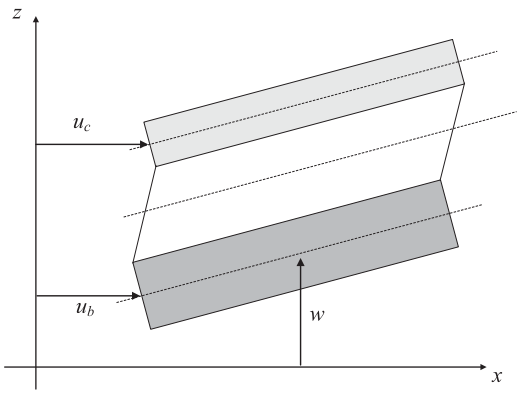

Fig. 6. Deformed element with displacements [5].

Laplace transform is used to write the Prony series in the Laplace domain [18,19]:

$$G^*(s) = G_0 - G_0 \sum_{n=1}^{N_p} g_n + \sum_{n=1}^{N_p} \frac{G_0 g_n \tau_n s}{1 + \tau_n s}, \tag{24}$$

where τ_n and g_n are the material specific parameters, $G_0 = G(t = 0)$ is the instantaneous relaxation modulus, and N_P is the number of terms required to properly describe the material. The storage modulus is given as $G_s = \mathrm{Re}(G^*)$ and the loss modulus is $G_l = \mathrm{Im}(G^*)$.

4.3. Equations of motion

The Lagrange's equations were used to derive the EOM of the PCLD beam, which was discretized using the assumed modes method [20]:

$$\mathbf{M}\begin{Bmatrix} \ddot{\boldsymbol{\psi}} \\ \ddot{\xi}_b \\ \ddot{\xi}_c \end{Bmatrix} + \mathbf{K}^*\begin{Bmatrix} \boldsymbol{\psi} \\ \xi_b \\ \xi_c \end{Bmatrix} = \begin{Bmatrix} \mathbf{Q}_\psi \\ \mathbf{0} \\ \mathbf{0} \end{Bmatrix}. \tag{25}$$

The generalized coordinates $\boldsymbol{\psi}$, ξ_b, and ξ_c are related to the beam displacements w, u_b, and u_c, respectively, through admissible functions [20,21]. The generalized force is given by $\mathbf{Q}_\psi = f(t)\mathbf{W}(x = x_f)$, where the actual impact force applied at $x = x_f$ is $f(x,t) = \delta(x - x_f)f(t)$.

The potential energy in the viscoelastic layer is due to shear stress. As a result of the complex shear modulus $G^*(s)$ introduced above, the potential energy (V_v^*) of this layer is also complex valued. The real part of V_v^* is actually strain energy, and the imaginary part is associated with energy dissipation. Therefore, the generalized stiffness matrix $\mathbf{K}^*$ is complex valued since it contains the frequency dependent viscoelastic shear modulus (G^*). The mass matrix $\mathbf{M}$ is real valued.

4.4. Solving for transient response

As discussed by Granger and Ross, the stiffness of the system is better represented in the frequency domain [5]. Therefore, it is more convenient to write the EOM (Eq. (25)) in the Laplace domain, i.e.

$$(\mathbf{K}^* + s^2\mathbf{M})\begin{Bmatrix} \overline{\boldsymbol{\psi}} \\ \overline{\xi_b} \\ \overline{\xi_c} \end{Bmatrix} = \begin{Bmatrix} \overline{\mathbf{Q}_\psi} \\ \mathbf{0} \\ \mathbf{0} \end{Bmatrix}, \tag{26}$$

where the overline symbol indicates a Laplace-transformed term which is a function of frequency ($s = \sigma + \mathrm{i}\omega$). A Dirac impulse $\delta(x - x_f)\delta(t)$ is applied in the Laplace domain, i.e. $\overline{\mathbf{Q}_\psi} = \mathbf{W}(x = x_f)$, to obtain the frequency response function for the transverse displacements of the beam, for an excitation load located at $x = x_f$. The actual forcing function $f(t)$ is Laplace-transformed using Eq. (21) and multiplied with the FRF to give the response of the beam in the Laplace domain. A Tukey window (Eq. (23)) and an inverse NLT (Eq. (22)) are then applied to obtain the time domain response $w(x,t)$ of the beam.

Table 2
Characteristics of the simulated beams.

	Base beam	Viscoelastic layer	Constraining layer
Material	Aluminum 3003	Urethane CPA-850	Aluminum 3003
Density (kg/m^3)	2710	1124	2710
Young's modulus (GPa)	70	–	70
Instantaneous relaxation Modulus (MPa)	–	14.1	–
Length (mm)	509	–	–
Width (mm)	25.4	25.4	25.4
Thickness (mm)	3.175	3.175	1.588

Table 3
PCLD configurations.

	Beam A	Beam B	Beam C
PCLD length (mm)	250	126	75
PCLD location (mm)	78	241	272

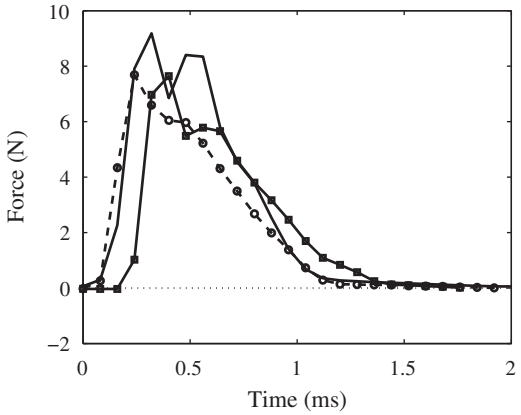

Fig. 7. Impact forces applied to Beams A (———), B (– ⊖ –), and C (—⊟—).

Table 4
Dynamic parameters of the viscoelastic layer.

n	g_n	τ_n
1	0.2	0.007
2	0.63	0.07

5. Results

Simulations were carried out to compare the Laplace transform method presented here with the Fourier transform method presented previously. Table 2 presents the constant parameters of the base beam, the viscoelastic layer and the constraining layer. Three cantilever beams were tested, each with a different PCLD configuration. In Table 3, all locations were measured from the clamped edge of the beam. PCLD location represents the distance from the clamp to the edge of the pad. Impacts were performed at 40 mm, and the displacements are given for a point located at 335 mm from the clamp. The impact force signals used were the same as presented by Granger and Ross [5] and are shown in Fig. 7. Parameters of the complex shear modulus of the viscoelastic layer (Eq. (24)) were obtained by using stress relaxation tests. The instantaneous relaxation modulus is given in Table 2, and the frequency dependent parameters are given in Table 4.

The simulation times for the Fourier and the Laplace approaches were 20 s and 25 ms, respectively. The time step was 0.04 ms in all simulations. Results from both the Laplace (———) and the Fourier (– ⊖ –) approaches are presented in Fig. 8 for Beam A, Fig. 9 for Beam B, and Fig. 10 for Beam C. Initial displacements are shown with respect to time for 22 ms after the beginning of the impact.

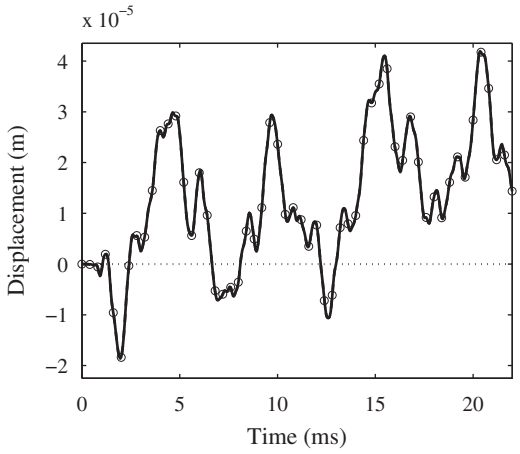

Fig. 8. Time response of impacted Beam A: inverse NLT (———) and inverse DFT (– ⊖ –).

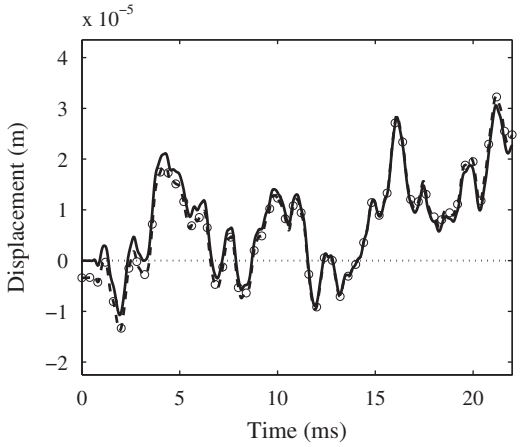

Fig. 9. Time response of impacted Beam B: inverse NLT (———) and inverse DFT (– ⊖ –).

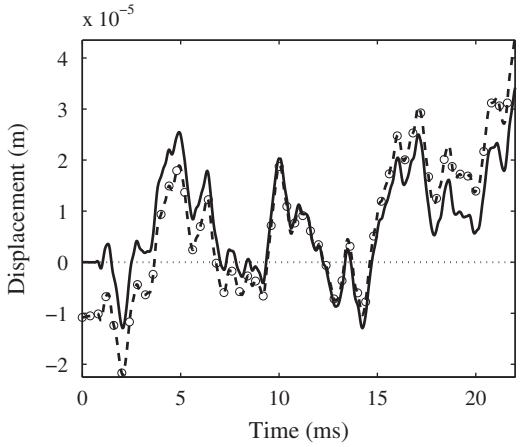

Fig. 10. Time response of impacted Beam C: inverse NLT (———) and inverse DFT (– ⊖ –).

Beam A is a fairly well damped beam. For this reason, the time response of the beam has died out inside the Fourier simulation window (20 s) and there is no error at time $t = 0$: there is no time aliasing and the response signal is causal. In this case, both the Fourier and the Laplace approaches yield exactly the same results in Fig. 8. Results for this type of

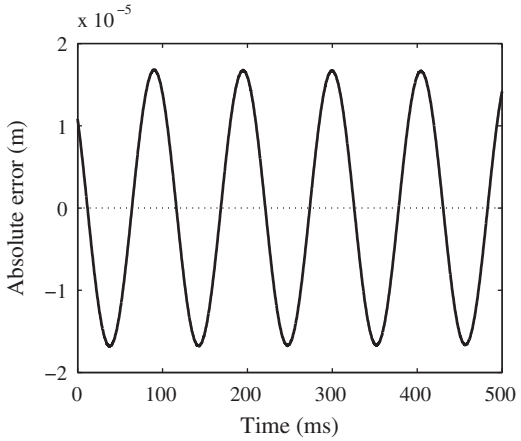

Fig. 11. Absolute error between the Fourier and the Laplace solutions, for Beam C.

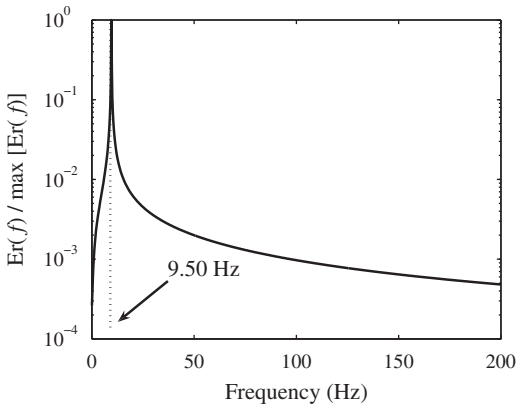

Fig. 12. Normalized error spectrum between the Fourier and the Laplace solutions, for Beam C.

configuration have previously been shown to be in very good agreement with experiments, and presented no visible causality error [5].

Beam B is a moderately damped beam. At the end of the Fourier simulation window, the displacements of the beam are sizeable ($-3.4\,\mu m$). In Fig. 9, the initial response at time $t = 0$ ms with the Fourier approach is also $-3.4\,\mu m$. This initial error is significant and corresponds to approximately 10 percent of the maximum displacement within the simulation window. Although the Laplace simulation window was 800 times shorter than the Fourier window, the results from the Laplace approach show no initial error. Except for the initial error in the Fourier calculations, which decreases regularly and seems to last for about 11 ms, the two signals are quite similar. Slight differences appear after 17 ms.

Beam C is a poorly damped beam. Displacements at the end of the Fourier simulation window ($-10.8\,\mu m$) are in the order of 48 percent of the maximum displacements. In Fig. 10, the initial error with the Fourier approach (also $-10.8\,\mu m$) is approximately 22 percent of the maximum displacement. Again, the results from the Laplace approach show no initial error. The two calculated responses are fairly similar in terms of peak location, but the amplitudes of the peaks are quite different. In this case, the discrepancies also diminish regularly and last for about 9 ms. However, discrepancies reappear increasingly around 15 ms and after, and reach a level similar to that observed at time $t = 0$. This is to say that aliasing seems to affect not only the very beginning of the signal, but possibly the entire signal.

In order to better understand the nature of the phenomenon, the absolute error of the Fourier solution with respect to the Laplace solution was plotted against time over 500 ms, for Beam C (Fig. 11). The error seems to be harmonic with a very low frequency. Its amplitude remains relatively constant throughout the observation window (about 4.5 cycles). It can therefore be stated that aliasing using the Fourier approach affects the response of the beam in an alternating way over a long time. To further study the error, its amplitude spectrum $Er(f)$ was normalized with respect to its maximum and was plotted in Fig. 12. The spectrum contains a very neat and narrow peak at 9.5 Hz. This value corresponds to the first natural frequency of the padded Beam C. In this beam, the first transverse mode is very little damped, since the PCLD is small and located far from the clamp. This mode is thus comparable to that of the single dof system used to describe aliasing in Section 2. Due to the discretization of the spectrum, the time response of this mode is being folded back to the beginning of

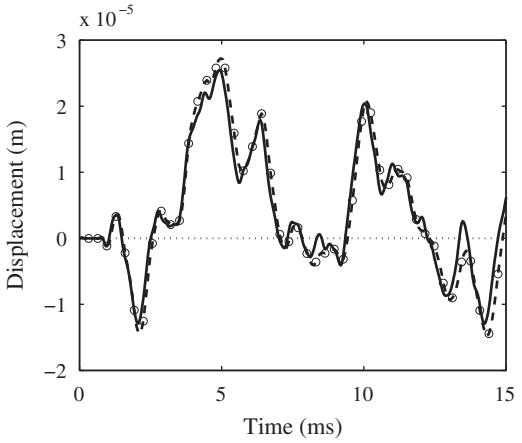

Fig. 13. Time response of impacted Beam C, calculated (———) and measured (– ⊖ –).

the time signal. In the present configuration, higher modes are less present in the impulse response, and are better damped than the first mode; therefore, their contribution to time aliasing is negligible.

6. Experimental validation

Experiments were carried out to validate the new solution method. Beam C was selected for this, since it is the one with the greatest aliasing error when using the Fourier approach. The impact conditions and force signals were obtained using an instrumented hammer. The duration of contact was about 1 ms. Displacements were obtained from an eddy current proximity probe. The sampling frequency for both the force and the displacement was 25 kHz ($\Delta t = 0.04$ ms). All testing conditions were identical to those described in Section 5.

The time response of Beam C was also calculated using the Laplace approach. The force signal measured on the experimental setup was used as the excitation force in the simulations. Fig. 13 shows the displacements obtained from the experiments (– ⊖ –) and from the simulation (———). Although Beam C is considered a worst case configuration, it can be seen that the simulated results are in excellent agreement with the experiments. No causality error can be observed. All peaks occur at the appropriate times, so no phase lag is observed. Some minor differences exist between the experimental and simulated responses, which are most likely due to experimental errors, and to the accuracy of the material properties used in the simulations.

7. Conclusion

In this paper, signal processing issues encountered when an analytical spectrum is converted in the time domain with an inverse discrete Fourier transform were discussed. It was shown analytically that the discretization of a continuous frequency spectrum leads to time aliasing and hence, to the noncausal effects previously observed by Granger and Ross. Moreover, time aliasing can cause considerable errors over the entire duration of the observation window, as it was shown with the numerical inversion of the FRF of a lightly damped system.

The numerical Laplace transform was introduced to suppress time aliasing, without requiring enormous simulation time as compared to the duration of the observation window. The real part of the Laplace variable was set to a constant value, so that the NLT and its inverse could be calculated using standard FFT algorithms. In counterpart, a Tukey window had to be used in the Laplace domain to avoid amplification of the Gibbs oscillations which were due to the truncation of the analytical spectrum.

The Laplace transform approach was applied to calculate the transient time response of impacted beams with a partial constrained viscoelastic layer. The results simulated over 25 ms showed that causality was perfectly respected, regardless of the amount of damping in the system. As a comparison, the Fourier approach solution proposed by Granger and Ross, and simulated over 20 s lead to causality errors worth up to 22 percent of the maximum displacement. The Laplace model and solution method are thus much more efficient than the Fourier approach, both from a computational point of view and for the quality of the results. Comparisons with experiments confirmed that modeling the system in the Laplace domain to calculate the transient displacements yielded excellent results.

It was discussed in previous work that the transient time response of an impacted mechanical structure contained valuable information on the system itself [5]. The present proposed model offers the opportunity to obtain the time response of the structure to any arbitrary excitation, regardless of the amount of damping. In future work, transmission and reflection of flexural and axial waves in each layer could be studied from a phenomenological point of view for a better

understanding of energy dissipation in viscoelastic materials. Such capability would greatly increase our ability to design vibration treatments for impacted structures.

Acknowledgments

This work was supported by the Natural Sciences and Engineering Research Council of Canada, the Fonds québécois de la recherche sur la nature et les technologies and the Institut de recherche Robert-Sauvé en santé et en sécurité au travail.

References

[1] J. Marcelin, P. Trompette, A. Smati, Optimal constrained layer damping with partial coverage, *Finite Element in Analysis and Design* 12 (1992) 273–280.
[2] E. Barkanov, Transient response analysis of structures made from viscoelastic materials, *International Journal for Numerical Methods in Engineering* 44 (3) (1999) 393–403.
[3] E. Barkanov, R. Rikards, C. Holste, O. Tager, Transient response of sandwich viscoelastic beams, plates, and shells under impulse loading, *Mechanics of Composite Materials* 36 (3) (2000) 215–222.
[4] M. Slanik, J. Nemes, M. Potvin, Time domain finite element simulations of damped multilayered beams using a Prony series representation, *Mechanics of Time-Dependent Materials* 4 (2000) 211–230.
[5] D. Granger, A. Ross, Effects of partial constrained viscoelastic layer damping parameters on the initial transient response of impacted cantilever beams: experimental and numerical results, *Journal of Sound and Vibration* 321 (1–2) (2009) 45–64.
[6] D.J. Wilcox, Numerical Laplace transformation and inversion, *International Journal of Electrical Engineering Education* 15 (3) (1978) 247–265.
[7] L.M. Wedepohl, Power systems transients: errors incurred in the numerical inversion of the Laplace transform, *Proceedings of Midwest Symposium on Circuits and Systems*, Puebla, Mex, 1983, pp. 174–178.
[8] A. Ramirez, P. Gomez, P. Moreno, A. Gutierrez, Frequency domain analysis of electromagnetic transients through the numerical Laplace transforms, *Proceedings of IEEE Power Engineering Society of America*, Denver, CO, USA, Vol. 1, 2004, pp. 1136–1139.
[9] W. Krings, H. Waller, Contribution to the numerical treatment of partial differential equations with the Laplace transformation—an application of the algorithm of the fast Fourier transformation, *International Journal of Numerical Methods in Engineering* 14 (8) (1979) 1183–1196.
[10] D.E. Beskos, A.Y. Michael, Solution of plane transient elastodynamic problems by finite elements and Laplace transform, *Computers & Structures* 18 (4) (1984) 695–701.
[11] H. Inoue, K. Kishimoto, T. Shibuya, K. Harada, Regularization of numerical inversion of the Laplace transform for the inverse analysis of impact force, *JSME International Journal, Series A* 41 (4) (1998) 473–480.
[12] Y.Q. Ni, W.J. Lou, J.M. Ko, A hybrid pseudo-force/Laplace transform method for non-linear transient response of a suspended cable, *Journal of Sound and Vibration* 238 (2) (2000) 189–214.
[13] D. Lévesque, L. Piché, A robust transfer matrix formulation for the ultrasonic response of multilayered absorbing media, *Journal of the Acoustical Society of America* 92 (1) (1992) 452–467.
[14] T. Nishigaki, T. Ohyama, M. Endo, Study of the transient sound radiated by impacted solid bodies based on the boundary element method, *JSME International Journal, Series C* 39 (2) (1996) 218–224.
[15] S.J. Day, N. Mullineux, J.R. Reed, Developments in obtaining transient response using Fourier transforms. I. Gibbs phenomena and Fourier integrals, *International Journal of Electrical Engineering Education* 3 (1) (1965) 501–506.
[16] E.G. Williams, *Fourier Acoustics, Sound Radiation and Nearfield Acoustical Holography*, Academic Press, San Diego, 1999.
[17] T. Pritz, Frequency dependencies of complex moduli and complex Poisson's ratio of real solid materials, *Journal of Sound and Vibration* 214 (1) (1998) 83–104.
[18] L. Rogers, A new algorithm for interconversion of the mechanical properties of viscoelastic materials, *AIAA Dynamics*, Palm Springs, USA, 1984.
[19] T. Chen, Determining a Prony series for a viscoelastic material from time varying strain data, Technical Report TM-2000-210123, NASA, 2000.
[20] S. Huang, D. Inman, E. Austin, Some design considerations for active and passive constrained layer damping treatments, *Smart Materials & Structures* 5 (1996) 301–313.
[21] H. Baruh, *Analytical Dynamics*, McGraw-Hill Science, Boston, 1999.